Experimental dynamic trapping of electrostatically actuated bistable micro-beams

Lior Medina,[1, a)] Rivka Gilat,[2] B. Robert Ilic,[3] and Slava Krylov[4]
[1)] *School of Mechanical Engineering, Faculty of Engineering, Tel-Aviv University, Ramat Aviv 6997801, Israel*
[2)] *Department of Civil Engineering, Faculty of Engineering, Ariel University, Ariel 44837, Israel*
[3)] *Center of Nanoscale Science and Technology, National Institute of Standards and Technology, Gaithersburg, MD, 20899, USA*
[4)] *Faculty of Engineering, School of Mechanical Engineering, Tel-Aviv University, Ramat Aviv 6997801, Israel*

(Dated: 12 February 2016)

We demonstrate dynamic snap-through from a primary to a secondary statically inaccessible stable configuration in single crystal silicon, curved, doubly clamped micromechanical beam structures. Nanoscale motion of the fabricated bistable micromechanical devices was transduced using a high speed camera. Our experimental and theoretical results collectively show, that the transition between the two stable states was solely achieved by a tailored time dependent electrostatic actuation. Fast imaging of micromechanical motion allowed for direct visualization of dynamic trapping at the statically inaccessible state. These results further suggest that our direct dynamic actuation transcends prevalent limitations in controlling geometrically non-linear microstructures, and may have applications extending to multi-stable, topologically optimized micromechanical logic and non-volatile memory architectures.

PACS numbers: 85.85.+j
Keywords: Curved micro-beam; Tailored electrostatic actuation; Dynamic trapping; Dynamic snap-through; Pull-in; MEMS/NEMS; High speed imaging; Dynamic bistability

Micro and nano electromechanical systems (MEMS and NEMS) comprising of bistable structural elements allow for two possible stable equilibrium configurations under identical external loading. These structures exhibit rich dynamical phenomena, have exquisite sensitivity near instabilities and allow for efficient control of deformed configuration using external fields. Collectively, these aspects give rise to a myriad of functional advantages in applications such as switches[1,2], sensors[3,4] and non-volatile memories[5]. The most common and widely used bistable element is a curved beam, shown in Fig. 1(a). The geometry of the beam is defined by its initial elevation h (defined as the distance between the center-point of the beam and the line connecting the clamped ends), thickness d, width b, and length L. The beam resides at a distance g_0 from an actuating electrode used to provide a distributed electrostatic load.

When actuated by a quasi-static electrostatic force, bistable beams exhibit two instabilities, namely a snap-through instability and an electrostatic, pull-in instability. Depending on the beam geometry, the critical snap-through voltage V_S, is either lower or higher than the critical pull-in voltage V_{PI}. Figure 1(b) shows the theoretically predicted dependence between the voltage and the beam midpoint elevation. On one hand, when $V_S < V_{PI}$, the beam snaps to its second stable equilibrium at the static snap-through voltage. On the other end of the spectrum, when $V_S > V_{PI}$, a voltage increase to V_S yields a response wherein the beam completely bypasses the second stable branch, thus making this stability point inaccessible under quasi-static actuation[6].

Suddenly applied step actuation leads to an outcome similar to that of the quasi-static case. For instance, a step actuation amplitude at the dynamic snap-through voltage V_{DS}, transfers the beam with $V_S < V_{PI}$ directly to the second stable branch. Prior to reaching the resulting stable state, the beam undergoes damped oscillations induced by the snap-through jump. Alternatively, the same actuation conditions coupled with $V_S > V_{PI}$ (and provided that $V_{DS} > V_{PI}$) yield a dynamic collapse of the beam to the electrode. However, as shown in this work, snap-through to a second, statically inaccessible stable equilibrium state is possible by applying a tailored time-dependent actuating signal[6]. Hereafter, for the sake of convenience, we refer to $V_S < V_{PI}$ for beams with a statically accessible second stable equilibrium as "bistable". Alternatively, beams distinguished by statically unreachable post-buckling stable configuration ($V_S > V_{PI}$) are referred to as "dynamically bistable".

Assuming a symmetric beam response, we employ a single degree of freedom model obtained using Galerkin decomposition to describe the beam dynamics[6]. The equation of motion is given by

[a)] Electronic mail: liormedi@post.tau.ac.il

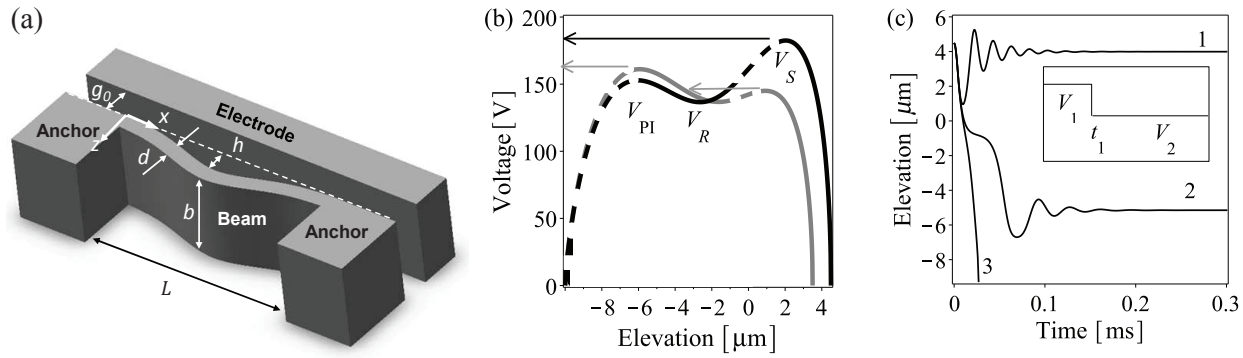

FIG. 1. (a) Schematic illustration of an initially curved beam under electrostatic actuation. (b) Predicted static equilibrium curves (a solution of the static counterpart of Eq. (1)) for two beams with $d=3.6$ μm and $g_0=10$ μm at different initial elevations of $h=3.5$ μm (gray) and $h=4.5$ μm (black). Arrows represent beam movement upon reaching V_S and V_{PI}. V_R corresponds to the snap-back release point and dashed lines represent unstable branches. (c) Calculated response of a dynamically bistable beam (black curve in (b)) to a sudden application of a two step signal (shown schematically in the inset), assuming a quality factor of $Q=5$, with $V_1=250$ V, $t_1=4$ μs and a varying V_2. Lines labeled (1), (2) and (3) correspond to V_2 values of 120 V, 150 V and 160 V, respectively.

$$\frac{3L}{8}\rho A\ddot{w}_m+\frac{3L}{8}c\dot{w}_m+\frac{2\pi^4}{L^3}\tilde{E}I_{yy}\left(w_m-h\right)+\frac{\pi^4}{8L^3}\tilde{E}A\left(w_m^2-h^2\right)w_m=-\frac{\epsilon_0 bV_a^2L}{4\sqrt{g_0\left(g_0+w_m\right)^3}} \tag{1}$$

with zero initial conditions $w_m(0)=h_0$, $\dot{w}_m(0)=0$, where ρ, $\tilde{E}$, A, I_{yy} and w_m are the beam density, effective (plain strain) modulus of elasticity, cross sectional area, moment of inertia and the beam midpoint elevation above the clamped ends, respectively. $\epsilon_0=8.854\times10^{-12}$ F/m is the permittivity of the free space, c is the damping coefficient, V_a is the actuation voltage and $\dot{(\,)}$ denotes the derivative with respect to time. Natural frequency of the curved beam, associated with the linearized version of Eq. (1) with $V_a=0$ and $hA\left(w_m-h\right)/I_{yy}\ll1$, is given by

$$\omega_n=\frac{\pi^2}{3L^2}\sqrt{\frac{2\tilde{E}}{\rho}\left(2d^2+3h^2\right)} \tag{2}$$

For the case of a straight beam, the frequency provided by eq. (2) differs from the exact value by 1.8 %.

The following time-dependent actuation scenario, suitable for dynamic bistability, involves a two-step (three parameters) loading[7]

$$V_a\left(t\right)=V_1H\left(t\right)-\left(V_1-V_2\right)H\left(t-t_1\right) \tag{3}$$

where H is the Heaviside step function. Inset of Fig. 1(c) illustrates the two step actuation process. At the onset, V_1 is suddenly applied and after a short time t_1, V_1 is reduced to a value of V_2. In order to escape the primary stable branch, the amplitude V_1 must be higher than V_{DS}, and t_1, should be within a certain range[6]. However, as shown in Figure 1(c), the overall actuation response depends strongly on V_2. Figure 1(c) further shows that at a moderate value $V_2<V_R$, the beam oscillates near its initial position (line 1). For an increased V_2, the beam snaps to the second stable state (line 2), and the highest $V_2>V_{PI}$ yields a pull-in (line 3). Our calculated results in Fig. 1(c) collectively confirm that beam trapping at the statically inaccessible branch requires V_2 values within the operational range of the second stable branch, i.e. $V_R<V_2<V_{PI}$ (see[6] for details).

TABLE I. Nominal and measured (in parentheses) dimensions of beams used in experiments.

Dimension	Beam 1 [μm]	Beam 2 [μm]
h_0 (h)	4 ($\sim$5.4)	4.5 ($\sim$4.9)
d	3.5 ($\sim$3.6)	3.5 ($\sim$3.2)
g_0	10 ($\sim$10.1)	10 ($\sim$10.4)

Devices were fabricated from a single crystal silicon on insulator wafer with a highly doped silicon device layer. The beams, characterized by a nominal width of 20 μm and length of 1000 μm, were lithographically defined, and subsequently etched using deep reactive ion etching (see[8] for details regarding fabrication). Geometric parameters of the resulting beams, primarily d, g_0 and the overall initial distance of the beam midspan from the electrode (g_0+h), were measured using an environmental scanning electron microscope (ESEM) with an error of ≈ 60 nm (one standard deviation). The estimated measurement error was based on the pixel to nm conversion factor of the ESEM image[9]. The difference between the nominal

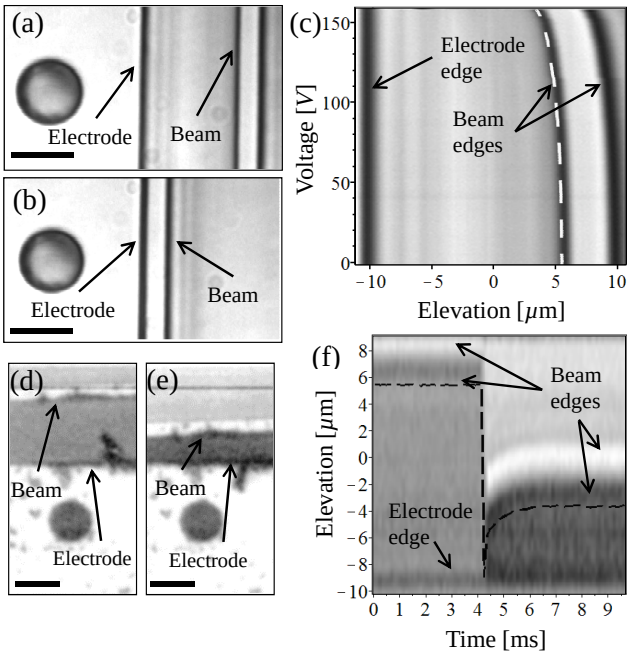

FIG. 2. Quasi-static (a)-(c) and dynamic (d)-(f) response of dynamically bistable beam 1 from Tab. I. Optical micrographs showing the (a) initial and (b) final positions of the curved beam following pull-in. (c) Direct visualization of the beam midpoint elevation w_m during actuation. Dashed white line represents the resulting buckling curve. (d) Initial beam position prior dynamic actuation. (e) Final position directly following dynamic trapping. (f) Direct visualization (at a frame rate of 9009 s^{-1}) of the beam midpoint elevation w_m and the resulting time history (dashed black line). The black scale bars in (a),(b),(d) and (e) represent 10 μm.

and actual measured dimensions of the beams, Table I, are due to the fabrication tolerances (e.g., see[9]).

The die was mounted on a wafer probing station operating at room temperature under ambient air conditions. The electrical signal was generated by a data acquisition card and amplified (×100) using a dual channel amplifier, giving an error of 0.1 V[10]. The in-plane (parallel to the wafer surface) motion of the beams was measured using an optical trinocular microscope in conjunction with a high speed camera. For our high speed acquisition measurements, we estimated a location error $\approx$0.227 μm. For static experiments, we used a high resolution, slower rate camera with an estimated displacement error of $\approx$ 90 nm. Both errors emanate from the pixel to μm ratio determined from the camera resolution and represent one standard deviation. Collected results consisted of an image sequence capturing the position of both the beam midspan and the stationary electrode (Fig. 2(c)). Images were analyzed using image processing procedures established in our earlier work[9].

In order to determine the primary stable branch of the buckling curve and the static snap-through voltage (V_S), each beam was first subjected to quasi-static loading[9]. Our results confirmed that all of the fabricated micromechanical beams were dynamically bistable. Following the static experiments, each beam was then subjected to dynamic actuation using a signal given by Eq. (3). By varying loading parameters, we experimentally observed all three possible response scenarios shown in Fig. 1(c). The appropriate values of t_1, V_1 and V_2 were found by trial and error using an initial guess based on the numerical solution of Eq. (1)[6]. Excessive loads gave rise to undesirable pull-in, wherein the beam undergoes stiction to the electrode. To recover and further use such a device, the beam was mechanically released from the electrode, thereby snapping back to its initially curved state.

Experimental quasi-static and dynamic results of the device designated as beam 1 from Tab. I, are collectively shown in Fig. 2. Using Eq. (2), for the measured beam geometry, the corresponding calculated natural harmonic was 68560.3 Hz. Optical micrographs in figures 2(a) and (b) show corresponding representative initial and final (pull-in) positions of the curved micromechanical beam. Direct visualization of the quasi-static response[11] shown in Figure 2(c) confirms the predicted ($V_S > V_{PI}$ case in Fig. 1(b)) pull-in behavior, with $V_S \approx 156$ V. Furthermore, prior to pull-in, the superimposed white dashed line in Fig. 2(c) shows the primary stable buckling curve.

Figures 2(d)-(f) show the experimentally measured dynamic response under a load described by Eq. (3) with $V_1 \approx 220$ V, $t_1 \approx 0.2$ ms and $V_2 \approx 110$ V. We readily observed transitions from the initial state (Fig. 2(d)) to the final stationary equilibrium (Fig. 2(e)). Black marks in Fig. 2(d) and (e) optical micrographs reflect damage generated from the pull-in impact experiments and subsequent mechanical release. Using a camera, sampling at a frame rate of 9009 s^{-1}, dynamic buckling behavior was directly visualized (Fig. 2(f)), clearly showing the transition from the initial to the stationary equilibrium state. This behavior is consistent with our predictions for $V_S > V_{PI}$ (case (2) in Fig. 1(b)). Furthermore, our dynamic analysis reveals that snap-through transition to the second equilibrium position is accompanied by fast oscillations. Our model shows that falling edge oscillations decay over a duration of $\approx$ 200 μs (Fig. 1(c)). Sampling at a frame rate of 9009 s^{-1}, this decay takes place over a duration of less than two frames ($\approx$222 μs). Since we are sampling at a rate slower than the Nyquist frequency, the full time history of the transient motion during snap-through can not be resolved. The slow ($\approx$ 2-3 ms), non-oscillating beam deflection decrease directly following snap-through is not captured by our model response. Checking the possibility that this can be attributed to the squeeze film damping, we found, using the simplest squeeze film model[12], that the latter yields a quality factor $Q \approx$145 in the first stable configuration, and $Q \approx 1.8$ at a second stable position. This corresponds to the decay time of several tens of μs, which is much shorter than $\approx$ 2-3 ms decay observed in our experiments, Fig. 2(f). We therefore attribute the deflection decay to possible discharging effects. The measured

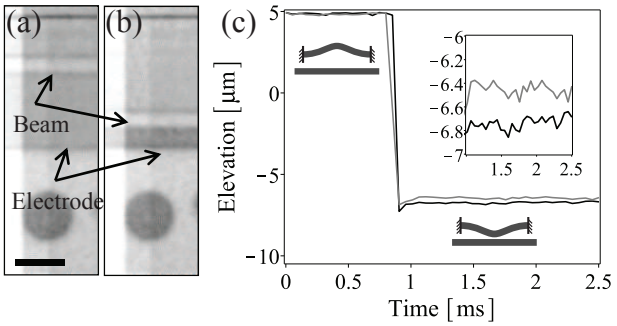

FIG. 3. (a), (b) Optical micrographs of the initial and post dynamic snap-through positions for beam 2 presented in Tab. I. The scale bar corresponds to 10 μm. (c) Time history curves for two distinct second step voltages V_2. The gray and black lines correspond to $V_2 \approx 111$ V and $V_2 \approx 112$ V, respectively. Inset illustrates the zoom-in of the final positions corresponding to two different V_2.

time history in figure 2(f) shows a trapped beam at the equilibrium point. Within the resulting stable state, the beam edge (the surface facing the electrode), resides at a distance of $\approx$6.5 μm from the electrode. Based on this position, the beam occupies $(h - w_m) / (h + g_0) \approx 58.2$ % of the gap. Further tailoring of the structural dimensions allows for a precisely engineered stable state within g_0.

Similar experiments were carried out for an additional beam with different geometry (beam 2, Tab. I), characterised by $\omega_n/(2\pi) \approx 61853.2$ Hz, and the measured static snap-through voltage of $V_S \approx 122$ V. The dynamic trapping, with $V_1 \approx 230$ V, $t_1 \approx 0.1$ ms and $V_2 \approx 112$ V, displaced the beam to a stable equilibrium state at a distance of $\approx$3.6 μm from the electrode, occupying $\approx$76 % of the gap. Direct visualization of the dynamic response was accomplished using a frame rate of 18779 s^{-1}. Figs. 3(a) and (b) show the corresponding frames of the initial and final positions, respectively and the ensuing time history is shown in black in 3(c).

The demonstrated dynamic trapping transfers the micromechanical beam to a stable equilibrium point on the second stable branch. Our experimental results further show that the position of the stable state is strongly dependent on V_2. Using identical conditions described previously for the second mechanical beam, a moderate adjustment of the second step to $V_2 \approx 111$ V, resulted in a position of $\approx$4 μm from the electrode, Fig. 3(c). Overall, a higher value of V_2 leads to a stability point closer to the electrode. In effect, the beam progresses further along its stable branch with increasing actuation voltage[9].

To summarize, we demonstrate snap-through of single crystal silicon beams to statically inaccessible stable equilibrium states, using a tailored two step actuation. By varying the actuating potential, we achieved control of the stability position. Furthermore, the potential V_2 required for positioning the beam at the second stable branch was lower than required for static and dynamic snap-through, allowing beam manipulation within close proximity to the electrode at moderate actuation voltages. Collectively, our experimental results are in reasonable agreement with model predictions. In contrast to static bistability ($V_S < V_{PI}$), the considerable tunability range of dynamic trapping extends applicability of bistable phenomenon to broad, technologically relevant applications. For example, topologically optimized micro and nanomechanical beams could provide the required network of accessible multi-stable states for non-volatile mechanical memory, and logic applications. Furthermore, the gap tunability feature renders these kinds of devices as beneficial in highly reliable, non-contact, capacitive or optical switching applications. The dynamic trapping phenomena, along with the approach to reach statically inaccessible stable states, is general in character and is applicable across many scientific disciplines including complex optical systems[13,14] and opto-mehcanical[1,15] that demonstrate bistabilty.

Acknowledgments. The authors would like to thank Erez Benjamin, Stella Lulinski and Yoav Linzon for their help with experiments and the staff at the Cornell Nanoscale Facility for generous aid in fabrication. The research was supported by the Broadcom Foundation, Tel Aviv University Authentication Initiative, Ariel University and Israel Ministry of Science, Technology and Space.

[1] V. Intaraprasonk and S. Fan, Applied Physics Letters **98**, article number 241104 (2011).
[2] F. K. Chowdhury, D. Saab, and M. Tabib-Azar, Sensors and Actuators A: Physical **188**, 481 (2012).
[3] D. R. Southworth, L. M. Bellan, Y. Linzon, H. G. Craighead, and J. M. Parpia, Applied Physics Letters **96**, article number 163503 (2010).
[4] R. Harne and K. Wang, Journal of Sound and Vibration **333**, 2241 (2014).
[5] B. Charlot, W. Sun, K. Yamashita, H. Fujita, and H. Toshiyoshi, Journal of Micromechanics and Microengineering **18**, article number 045005 (2008).
[6] L. Medina, R. Gilat, and S. Krylov, Communications in Nonlinear Science and Numerical Simulation **36**, 273 (2016).
[7] V. Leus and D. Elata, Microelectromechanical Systems, Journal of **17**, 236 (2008).
[8] S. Krylov, B. Ilic, D. Schreiber, S. Seretensky, and H. Craighead, Journal of Micromechanics and Microengineering **18**, 055026 (2008).
[9] L. Medina, R. Gilat, B. Ilic, and S. Krylov, Sensors and Actuators A: Physical **220**, 323 (2014).
[10] *Model PZD350A M/S, Piezo Driver/Amplifier Series - Data sheet*.
[11] Y. Gerson, I. Sokolov, T. Nachmias, B. Ilic, S. Lulinsky, and S. Krylov, Sensors and Actuators A: Physical **199**, 227 (2013).
[12] S. Krylov, International Journal of Non-Linear Mechanics **42**, 626 (2007).
[13] M. Bagheri, M. Poot, M. Li, W. P. Pernice, and H. X. Tang, Nature nanotechnology **6**, 726 (2011).
[14] E. Bulgakov, A. Sadreev, and K. N. Pichugin, in *Spontaneous Symmetry Breaking, Self-Trapping, and Josephson Oscillations* (Springer, 2013) pp. 89–124.
[15] B. Dong, H. Cai, L. Chin, J. Huang, Z. Yang, Y. Gu, G. Ng, W. Ser, D. Kwong, and A. Liu, Applied Physics Letters **107**, 261111 (2015).